Pulse shaping and characterization of spectra exceeding one octave

José Ricardo Cardoso de Andrade

Grupo de lasers e Plasmas, Instituto de Plasmas e Fusão Nuclear, Instituto Superior Técnico (IST), Lisbon, Portugal

Ultrafast Optics Group, Institut für Quantenoptik, Leibniz Universität Hannover (LUH), Hanover, Germany

Under supervision of Dr. Gonçalo Figueira (IST), Dr. Anne Harth (LUH) and Prof. Uwe Morgner (LUH)

September 2013

Abstract

The development of ultra-broadband mode-locked laser sources has experienced a significant progress over recent years. This evolution leads to a corresponding need for the development of adequate pulse shaping, compression and spectral phase characterization schemes. This work provides a detailed analysis of a linear shaping setup by the use of a spatial light modulator in a 4-f prism-based geometry as a compression scheme for lasers with spectra spanning over one octave. This setup was applied to a two-color pumped parametric chirped-pulse-amplifier extending from 430 nm to 1.3 μm. Calibration and usage procedures are explained, as well as a thorough exposition of the limitations of the setup, which are currently preventing an effective compression of the purposely highly chirped laser output. Since the pulse has a Fourier transform-limited duration of $\sim$2.5 fs supporting a 1.2 cycle pulse, a brief overview on CEP stabilization is performed and a locked CEP is experimentally demonstrated. We review broadband spectral phase retrieval methods, in particular SPIDER, MIIPS (along with simulations) and d-scan. Their implementation, pros and cons are also discussed.

1 Introduction

Ultra-broadband mode-locked lasers, that easily span more than one octave are becoming easier to build due to the evolution of laser optics and the understanding of nonlinear phenomena. Such lasers have several important scientific and technological applications such as high harmonic generation (HHG) [1] and spectroscopy [2]. However, dispersion effects considerably more noticeable for such pulses, broadening their duration by a large factor.

Existing mainstream compression methods, such as pairs of diffraction gratings [3, 4] or prisms [5] have been developed more than two decades ago, when state-of-the-art ultrashort laser pulses were not so broadband. This calls for a need to investigate and develop new, ultrabroad compression methods, or, to adapt the currect devices for the new generation of ultrashort pulses. On the other hand, spectral phase characterization methods are seldom well adapted to pulses near the single-cycle regime either.

There are three widely spread compression schemes. Prism pair compression [5], grating based compressors [3, 4] and the use of dispersion compensation mirrors (DCMs) [6]. Prism pairs do not perform well when applied to systems spanning well over once octave, beacause the conjugation of two prisms introduces higher-order dispersion on a broadband spectrum, which creates unwanted temporal artifacts, such as pre- or post-pulses and envelope modulations. Grating based compression schemes are ruled out for the single fact that for a source that spans above once octave, two diffraction orders will overlap in space, making them impossible to use. For single-stage laser systems, such as used in the present work, there is the additional issue of low efficiency. Since there is no amplification stage following the compression, the output energy would be significantly decreased. Finally, even though technology has come a long way since their first development, dispersion compensating mirrors are still unable to provide a target group delay dispersion (GDD) while ensuring a high reflectivity: these two desirable characteristics are still mutually exclusive for lasers spanning over one octave.

In this work, we describe the adaptation of a spatial light modulator (SLM) in a 4-f prism based shaper [7, 8] to compress pulses that span over one octave. This method is able to compensate higher-order dispersions, making it more versatile; has low energy losses due to the nonexistent gratings; and after compression, it can be used as a shaping tool, which can be used to change several important parameters such as carrier-envelope phase, or polarization.

For characterization of the spectral phase, two different methods – better adapted to ultra-broadband spectra than SPIDER [9] or FROG [10] – are presented: MIIPS [11] (along with simulations) and d-scan [12, 13].

Both the compression and characterization methods are applied to a 1.5 octave spanning two-color pumped optically parametrically chirped pulse amplified (OPCPA) system which has a Fourier limit of 2.5 fs at FWHM [14].

1.1 Pulse shaping using a spatial light modulator

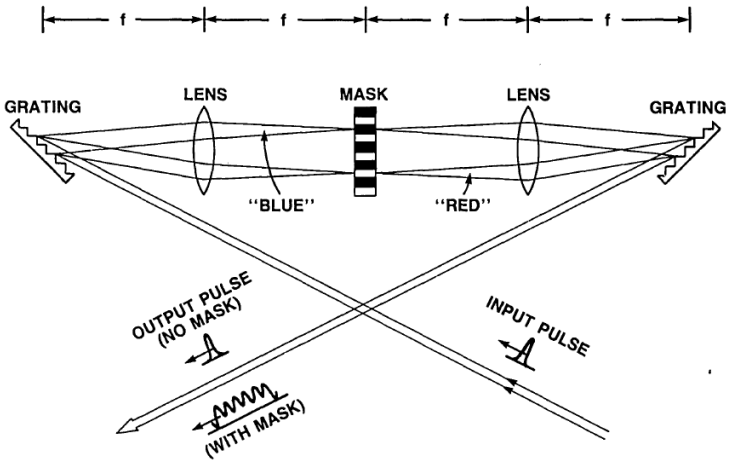

Figure 1: Depiction of a 4-f shaping apparatus (grating based). The SLM is positioned in the masking plane (from [15]).

Figure 1 shows a typical 4-f pulse shaping setup. This designation comes from the geometry of the setup, whose total length is four focal lengths f of the used lens (or curved mirrors, as in the case of our setup – Appendix, Fig. 6).

Pulse shaping takes advantage of the spatially dispersing elements such as gratings, to be able to modulate the individual frequency components of a laser pulse in the Fourier plane. In this plane a mask is being used to transfer a desired modulation to the laser pulse. This is a time-invariant filter technique – also widely used in electronics, such that the output pulse in the time domain $e_{\text{out}}(t)$ is given by the convolution:

$$e_{\text{out}}(t) = e_{\text{in}}(t) * h(t) = \int e_{\text{in}}(t') \cdot h(t - t')dt', \tag{1}$$

where the time-invariant filter is given by a time response function $h(t)$ that is applied to the input pulse $e_{\text{in}}(t)$. In the frequency domain, the output $E_{\text{out}}(\omega)$ is given by multiplying the input pulse $E_{\text{in}}(\omega)$ and the filter $H(\omega)$ in the frequency domain:

$$E_{\text{out}}(\omega) = E_{\text{in}}(\omega)H(\omega). \tag{2}$$

This is a much more convenient way to express the shaping process. $H(\omega)$ should mimic exactly the intended filtering in the frequency domain, and it is indeed, what is applied at the masking plane of the apparatus. This mask has a frequency-dependent complex transmittance and in the case of our setup, as we were using a liquid crystal SLM to apply the mask, it is discretized into 640 elements (pixels). Each element is a combination of two liquid crystal cell, where each cell is addressed individually in order to impose a voltage dependent phase delay. This makes it possible to impose either just a phase or an amplitude modulation by using polarizers before and after the device.

The discretization of the mask, the finite width of the beam radius (for a Gaussian shaped beam, defined as the radial distance at which the electric field amplitude decays to $1/e$ of that at the axis) $w_0(\omega)$ (for ultra-broadband spectra this parameter depends on the frequency ω, although for small focal distances f this value can be approximated to a constant) and the spatial distribution of the frequencies on the masking plane $\alpha \equiv \partial x/\partial\omega$ have effects on the time output, changing the effectiveness of the time-invariant filter:

$$e_{\text{out}}(t) = e_{\text{in}}(t) * \left(\tilde{s}_{\text{eff}}(t) \cdot \text{sinc}\left(t\frac{\delta_\omega}{2} \right) \cdot e^{-w_0^2 t^2/8\alpha^2} \right), \tag{3}$$

where δ_ω is the difference in orbital frequency between two neighbouring pixels, the sinc() function is defined by $\sin(x)/x$ and the effective wanted time profile $\tilde{s}_{\text{eff}}(t)$ is given by:

$$\tilde{s}_{\text{eff}}(t) \approx \sum_m \tilde{s}(t - m\delta_f^{-1}), \tag{4}$$

which means that the effective time waveform is a series of self-replicas separated by δ_f^{-1} where δ_f is the frequency difference between two adjacent pixels. These time replicas are attenuated by the sinc() function of Eq. (3) which only dependens on $\delta_\omega = 2\pi\delta_f$.

The most important parameter in Eq. (3) is the FWHM of the Gaussian envelope (last term) which gives the time window:

$$\Delta T = \frac{4\alpha\sqrt{\ln 2}}{w_0}, \tag{5}$$

where shaping is possible. This means that for delay times outside this shaping window, the output intensity will be too low (or even zero). If the beam size is too small, the temporal window is large, but the shaped waveform will have many replicas as given by Eq. (4), which is also undesirable as it means that energy is being diffracted to other modes.

We may now define a resolution η which gives the number of features that are possible to shape inside this temporal window, given by:

$$\eta = \frac{\Delta T}{\Delta t}. \tag{6}$$

Here Δt is the FWHM of the transform limited pulse, set by the full bandwidth incident on the shaper. Eqs. (5) and (6) show that the resolution can be tuned by tuning of the spatial distribution α and the beam radius w_0.

2 Laser source

The compression setup and characterization method presented in this work are applied to a two-color pumped optical parametric chirped pulse amplifier (OPCPA) system which has an output spectrum spanning from 430 nm to 1.3 μm (Figure 2(a)) with a Fourier limit of ~2.5 fs at FWHM (Fig. 2(b)). All the details of the system may be found in Ref. [14].

The laser is being used at a repetition rate of ~200 kHz – but can be tuned in a range from 100 kHz to 500 kHz which also changes the output power. The energy per pulse is of 1 μJ.

2.1 CEP stabilization

The output of the laser has the potential of a near single-cycle output, meaning that the carrier-envelope phase (CEP) is an important parameter, to perform experiments with this system. With that in mind,

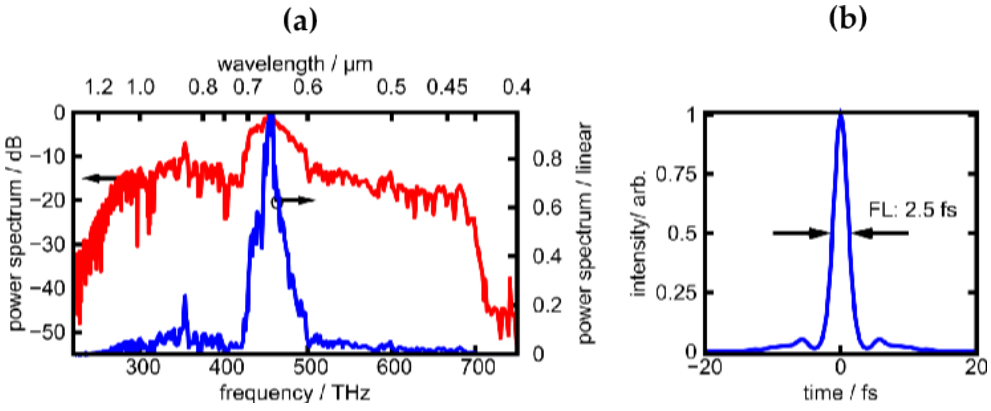

Figure 2: Output spectrum of the laser source and corresponding Fourier limit. (a) Spectrum in dB as red and as linear scale in blue. (b) Transform limit of such spectrum. Under the envelope there is a 1.2 cycle of the electric field at the central wavelength 650 nm.

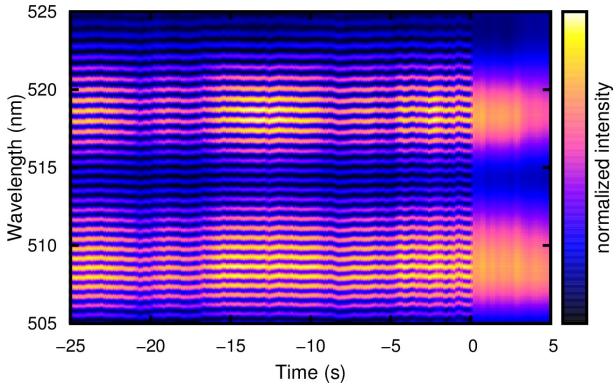

Figure 3: Time scan of the spectral output of an f-2f interferometer after the 1st NOPA stage and a white-light continuum generation. The lock to 0 frequency of the CE slippage is evident. At the 0 s mark, the locking electronics at the oscillator are turned off. Each time slot holds an interference of more than 10^4 pulses.

the seed oscillator of the subsequent non-collinear optical parametric amplifiers (NOPA) is optionally CEP slippage stabilized. With the aid of an acousto-optical modulator and electronics the oscillator CE frequency is stabilized to a quarter frequency of its own repetition rate. By amplifying every 4th pulse of the seed pulse train at the first NOPA stage, there is the insurance of a locking of the CE frequency to 0 Hz.

This was tested after the 1st NOPA stage and the creation of a supercontinuum in a sapphire plate. As it was demonstrated that there is a lock to 0 after these two processes, phase properties would also be maintained after the second NOPA stage and so, it is possible to maintain a 0 Hz carrier-envelope slippage. A time scan of the spectral output of an f-2f interferometer can be seen in Figure 3.

Although the locking of the phase to zero was demonstrated, the phase rms value is still quite poor as shown by the ripples in the interference scan of Fig. 3. There is still room for improvements by the use of a second locking system after the output, to ensure a very stable and truly zero CE frequency locked system.

3 Compression: 4-f and prism based shaper

As mentioned in the introduction, a shaping apparatus using an SLM (spatial light modulator) in a 4-f prism based geometry was implemented as means of compression of the spectrum of the above mentioned laser. This would also ensure a versatile tool in terms of shaping, after the achievement of a near transform-limited pulse.

3.1 Shaping apparatus for the two-color pumped OPCPA

In order to use the above mentioned scheme to compress/shape a source that spans more than one octave, the gratings need to be replaced by another spatially dispersive element, as the overlap of two diffraction orders makes them unusable. In the case of the source used in this work, the gratings were replaced by an F2 Schott glass prism, and the whole setup was used in a folded geometry (a mirror is placed after the SLM such that the pulse back-propagates through the same path – Appendix, Fig. 6). Binhammer

et al. [8] showed it to be a powerful tool both as compressor and as shaper for an octave spanning laser. Nevertheless, they use prism pairs as a pre-compensation of the dispersion imparted by the prism. In the case of this work, this was ruled out due to the higher-order dispersion features that would arise from this procedure and would be impossible to eliminate, as the spectrum spans for 1.5 octaves.

The following analysis consists of theoretical calculations of the shaper parameters used in this work, and they reflect the needed effort to compress the dispersion introduced by the prism.

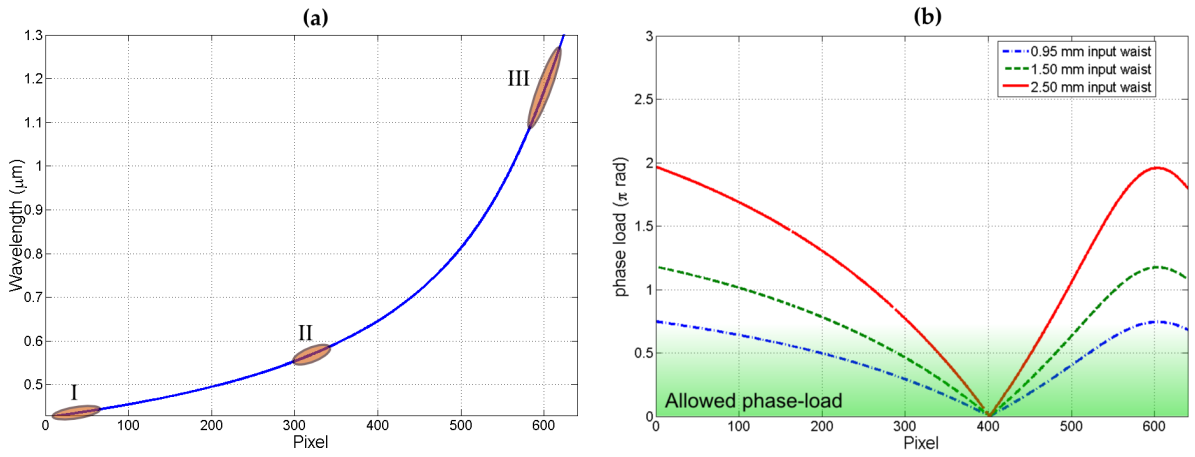

Figure 4: Theoretical curves of the spatial distribution of wavelength along the masking plane and of the phase-load for different incident beam radii. (a) Wavelength distribution along the masking plane with three 40-pixel-wide marked zones. Each zone is centered as follows: 40th pixel for I; 320th pixel for II; and 580th pixel for III. (b) Phase-load for different input beam radii: solid red of 2.5 mm; dotted green of 1.5 mm; and dashed blue of 0.95 mm. Phase-load is the phase difference between two neighbouring pixels.

Figure 4(a) shows how the distribution of the full spectrum looks like when using the F2 prism. As expected, the distribution is not linear, because the optical anisotropy is not either. The three marked regions will be analyzed shortly. Each corresponds to 40 pixel-wide zones, where – by the application of the equations introduced in Section 1.1 – a quantitative and qualitative analysis is made. Figure 4(b) depicts the phase-load for different input beam radii. Phase-load is the phase difference between neighbouring pixels, when trying to compress the dispersion of the prism. It is directly related to the total dispersion on the beam, as a higher step in phase means that more dispersion needs to be compensated for. There is a difference of the phase-load for different input radii, because a wider beam size increases the travelled distance inside the prism. Phase-load should be well under π due to diffraction and destructive interference appearing for high values of the phase-load. A π phase difference results in a spectral hole and energy losses. A high value diffracts light into higher spatial modes as well as out of the main beam path. Although increasing the input beam radius increases dispersion, it also increases the resolution, because then the focal point at the masking plane is smaller.

A summary of the shaper parameters is given in Table 1. There, it is possible to see how the resolution η increases for larger input beam radii, while the beam radii at the focal plane w_0 becomes smaller. The value τ is directly linked to the phase-load by $\tau = |\delta_\varphi / 2\pi\delta_f|$. It represents the time displacement for a certain phase-load (in the table the used values were the averages of each zone). The pixel is where the

Table 1: Calculated values for the three zones shown in Fig. 4(a) and for three different input radii for prism compensation. The formulas are shown in the text as well as the analysis of the table.

				τ (fs)			
	w_{in} (mm)	w_0 (mm)	η	40th pixel	320th pixel	600th pixel	$\Delta T/2$ (fs)
I	0.95	0.140	33.81	47.36	608.10	1127.50	415.08
	1.50	0.087	54.40	74.78	960.16	1780.26	667.95
	2.50	0.052	90.94	124.63	1600.26	2967.10	1116.55
II	0.95	0.171	28.38	658.04	21.61	517.60	214.65
	1.50	0.105	45.92	1039.00	34.13	817.26	347.32
	2.50	0.063	76.83	1731.67	56.88	1362.10	581.03
III	0.95	0.361	14.61	1155.27	500.99	17.51	66.10
	1.50	0.205	25.75	1824.11	791.03	27.64	116.53
	2.50	0.121	43.47	3040.18	1318.39	46.07	196.69

phase was chosen to be zero, or where it was defined the time $t = 0$. The last parameter is half of the time window ΔT, i. e. the actual maximal value for which one is able to displace components.

To conclude that the shaper cannot compensate even for its own dispersion (introduced by the prism), one needs to compare the values of the τ columns with $\Delta T/2$. Each column of τ gives a distinct situation: the needed time displacement of the frequency components of each zone to compensate the broadening caused by the prism. Being the last column the maximum displacement that the shaper can impart to each zone, one notices that for the three different zero point cases, there is only one zone (the one where the zero phase was defined for) where the frequency components can be displaced to $t = 0$ (compensated for).

Zone III is the least favorable zone, where the spatial distribution of the different frequency components is low (there is not a significant chromatic separation) and the time window is very small, meaning that the best choice would be to place the $t = 0$ to that point. But the pulse is already too dispersed and the other two zones are already out of their time capabilities. In any way that one looks at this table, it is concluded that the shaper cannot compress the dispersion imprinted by the prism.

4 Characterization methods

Although widespread, SPIDER [9] and FROG [10] are not the best suited characterization methods when dealing with ultra-broadband lasers near the single-cycle limit. For these cases there are either different arrangements of the original SPIDER/FROG techniques or other techniques. For the present work only multiphoton intrapulse interference phase scan (MIIPS) [11] and d-scan [12, 13] are considered. The first one, due to the fact that an SLM based shaper can be used to iteratively characterize and compress a pulse. The second, because it has a robust retrieval algorithm and easy setup.

4.1 MIIPS

MIIPS is a technique that uses an SLM to impose a series of masks on the spectrum while recording the harmonic spectrum. The masks are done in a way that each frequency component of the spectrum gets a different amount of GDD. Then, as the masks are scanned across the spectrum, every frequency

ends up having a different GDD at every point of the scan. This ensures a full sampling. This procedure allows one to find what is the group delay dispersion (GDD) of a certain frequency, because the harmonic intensity I of a certain frequency ω_i depends on the GDD and it is maximum when the GDD of that frequency is 0 [16]:

$$I_{\max}(n\omega_i) \rightarrow \phi''(\omega_i) = \varphi''(\omega_i) + \phi''_{\mathrm{m}}(\omega_i) \approx 0,$$

where n is the harmonic order, $\phi'' = \partial^2\phi/\partial\omega^2$ is the total GDD of the pulse at the non-linear media, φ'' the unknown GDD of the measured pulse and ϕ''_{m} the GDD of the mask. This means that by knowing the exact GDD of each mask and recording where the harmonic spectrum intensity is maximum, it is possible to know what is the GDD of the frequency to which the maximum was recorded: $\varphi''(\omega_i) = -\phi''_{\mathrm{m}}$. After having a complete set of the GDD at each point, the spectral phase is retrieved by performing a double integration.

The retrieved phase is then inverted and fed to the SLM for pulse compression and the process is repeated if needed, to better approximate the real spectral phase.

In the case of the laser source of this work, the second harmonic cannot be used due to the overlap of fundamental and harmonic spectra. To solve this problem, thin films [17] can be used to create the third harmonic, without bandwidth limitations.

This technique has the advantage of being quite simple to implement if the setup already uses an SLM, and the retrieval procedure is straightforward, although, for some complex phases, there is the need of several iterations which may take several minutes.

The main issue of this technique is the failure of the retrieval mechanism for very complex spectral phases, specially if they have oscillatory features. This is due to the fact that for an accurate retrieval, MIIPS needs to have an intensity maximum for a certain frequency ω_i in one of the masks, otherwise it will not be sampled, and also because if the phase oscillates there will be two or more maxima for a single mask, and only one can be resolved.

4.1.1 Simulations

Several simulations were done to test a retrieval algorithm, and an example can be seen in Figure 5. Fig. 5(a) shows the first approximate GDD retrieval, and although not perfect, this is an iterative algorithm, that slowly approaches the exact value. Fig. 5(b) depicts the residual phase after the 4th iteration. This phase would achieve a pulse almost indistinguishable from the transform limited one.

4.2 D-scan

D-scan stands for dispersion scan and it is based in the same harmonic response effect as MIIPS. D-scan does not need an SLM and instead of a series of masks, it uses glass wedge insertion as a means of changing dispersion (Appendix, Fig. 7). The pulse is overcompensated dispersion-wise, by the use of doubly-chirped mirrors, and after the scan of glass wedge insertion is done and the harmonic response recorded, it is possible to both characterize the pulse and find which point of wedge insertion gives the shortest pulse. So it can be said that this technique both characterizes and compresses a pulse.

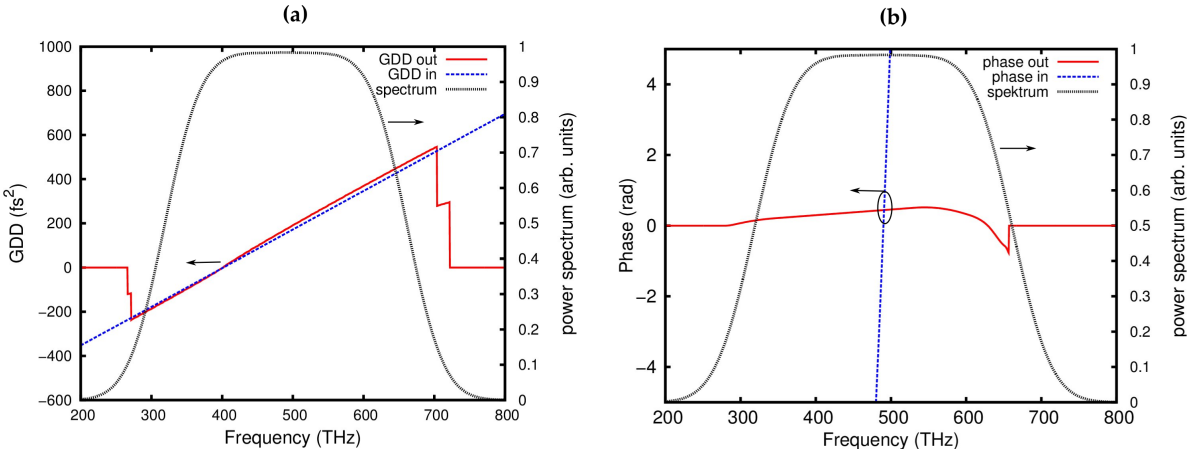

Figure 5: Simulations of MIIPS algorithm applied to a dummy spectrum. (a) Retrieved GDD after the first iteration, where input GDD is in dashed blue, retrieved GDD in solid red and the spectral intensity in dotted black. (b) Residual phase after the 4th iteration, with the input phase (scale too small to view completely) as dashed blue, retrieved phase as solid red and spectrum as dotted black.

The strong point of d-scan though, is the retrieval mechanism, where the experimental trace $S_{\mathrm{exp}}(\omega, \iota)$ – where ι is the inserted wedge thickness – is numerically compared to a theoretical one calculated from the fundamental spectrum $S_{\mathrm{calc}}(\omega, \iota)$. By fulfillment of

$$S_{\mathrm{exp}}(\omega, \iota) = \mu(\omega) \cdot S_{\mathrm{calc}}(\omega, \iota), \tag{7}$$

the phase has been well extracted. $\mu(\omega)$ is an intensity correction term which does not depend on wedge insertion, meaning that it has all the setup variables such as component transmission, nonlinear optical susceptibility $\chi^{(n)}(\omega)$ of the recorded harmonic of order n, etc.

This means that d-scan has no trouble retrieving more complex phases and it does not need to have a certain frequency ω present in the scan to be able to retrieve its phase, as it is encoded in the whole scan. However, d-scan needs to cross a near zero GDD point for the whole spectrum for a successful retrieval. Nevertheless, by the use of an SLM, this problem is easily overcome, as masking can create unique patterns that do not create ambiguities.

Like every other characterization technique that uses a nonlinear process, phase-matching is also an issue, and again, in the case of the used laser, the ultra-broadband spectrum can be well sampled (as well as have the harmonic separated from the fundamental) by performing the third harmonic generation in thin films.

5 Conclusions and outlook

5.1 Conclusions

In this work, a two-color pumped OPCPA system able to deliver an ultra-broadband spectrum that spans from 430 nm to 1.3 μm with a pulse energy of 1 μJ at a repetition rate of 200 kHz was demonstrated. It is optionally CEP stabilized, and it was also experimentally demonstrated.

Secondly, a comprehensive guide to shaping and compression of ultra-broadband spectra, that spans over one octave, through the use of an SLM in a 4-f geometry, is given. This shows the several limitations and engineering efforts that need to be considered for its application. Ultimately, it is shown that at the present, the use of this kind of shaping apparatus – at least with the used F2 glass prism – cannot compress the pulse of the above mentioned system.

Lastly, regarding characterization techniques of the spectral phase for near single-cycle pulses, pros and cons of SPIDER, MIIPS and d-scan were discussed. Implementation and usage is also described, as well as issues needed to be considered for ultra-broadband spectra.

5.2 Outlook

Non-collinear optical parametric amplification is still far from its limit and energy scalability should be the next step for the presented system, after a short pulse has been achieved. This will lead to new grounds for atto-science and laser development.

When it comes to shaping and characterization, for the fulfillment of the objective of compressing the pulse of the two-color pumped OPCPA, several approaches should be investigated. Namely, breaking the 4-f geometry; search for a different prism (material and apex angle); alternative pre-compensation scheme, for the dispersion imparted by the prism; and only if no other technique seems viable, separate the spectrum into two parts, and use a pulse synthesis technique to compress each spectral part independently.

Regarding characterization methods, the use of non-linear crystals will be mandatory for such broadband sources, meaning that phase-matching is an issue. This provides a way to help the development and characterization of better non-linear materials (e.g. non-linear thin films) that then can be applied in characterization methods providing unlimited bandwidth conversion.

To conclude, as pulses are being more and more broadband, the necessity of better and more reliable characterization and compression schemes for really short pulses pushes the investigation of new techniques.

The presented laser system was developed by the ultrafast optics group of Leibniz Universität Hannover, Hanover, Germany and it is installed in the same university, also where the entirety of the described work was performed.

Apart from the laser system and CEP stabilization, the rest of the work here presented was done by the author: implementation, calibration and theoretical predictions of the 4-f prism and SLM based shaper; MIIPS algorithm and simulations; out-of-loop f-2f interferometer for CEP stabilization proof.

Part of the work developed for this thesis was presented in two poster sessions: at German Physical Society (DPG) Spring Meeting (Frühjahrtagung) conference, Hanover, March 2013 with the title *Pulse compression and characterization of spectra supporting nearly single cycle pulses in the visible*; and CLEO/Europe conference, Munich, May 2013 with the title *4-f prism-based pulse shaper supporting single-cycle pulses in the visible*. A third poster has been approved for the ASSP conference, Paris, October 2013 with the title *Towards characterization and compression of a 1.5 octaves spectrum spanning from VIS to IR from a two-color pumped OPCPA system*.

References

[1] Lewenstein, M., Balcou, P., Ivanov, M. Y., L'Huillier, A., and Corkum, P. B. *Phys. Rev. A* **49**, 2117–2132 Mar (1994).

[2] Holzwarth, R., Udem, T., Hänsch, T. W., Knight, J. C., Wadsworth, W. J., and Russell, P. S. J. *Phys. Rev. Lett.* **85**, 2264–2267 Sep (2000).

[3] Treacy, E. *Quantum Electronics, IEEE Journal of* **5**(9), 454–458 (1969).

[4] Martinez, O. *Quantum Electronics, IEEE Journal of* **23**(1), 59–64 (1987).

[5] Fork, R. L., Martinez, O. E., and Gordon, J. P. *Opt. Lett.* **9**(5), 150–152 May (1984).

[6] Kaiser, N. and Pulker, H. K. *Optical Interference Coatings*, chapter Interference Coatings for Ultrafast Optics, 393–422. Springer (2003).

[7] Weiner, A. *Review of Scientific Instruments* **71**(5), 1929–1960 (2000).

[8] Binhammer, T., Rittweger, E., Ell, R., Kartner, F., and Morgner, U. *Quantum Electronics, IEEE Journal of* **41**(12), 1552–1557 (2005).

[9] Iaconis, C. and Walmsley, I. *Opt. Lett.* **23**(10), 792–794 May (1998).

[10] Kane, D. and Trebino, R. *Quantum Electronics, IEEE Journal of* **29**(2), 571–579 (1993).

[11] Lozovoy, V. V., Pastirk, I., and Dantus, M. *Opt. Lett.* **29**(7), 775–777 Apr (2004).

[12] Miranda, M., Fordell, T., Arnold, C., L'Huillier, A., and Crespo, H. *Opt. Express* **20**(1), 688–697 Jan (2012).

[13] Miranda, M., Arnold, C. L., Fordell, T., Silva, F., Alonso, B., Weigand, R., L'Huillier, A., and Crespo, H. *Opt. Express* **20**(17), 18732–18743 Aug (2012).

[14] Harth, A., Schultze, M., Lang, T., Binhammer, T., Rausch, S., and Morgner, U. *Opt. Express* **20**(3), 3076–3081 Jan (2012).

[15] Weiner, A. M., Heritage, J. P., and Kirschner, E. M. *J. Opt. Soc. Am. B* **5**(8), 1563–1572 Aug (1988).

[16] Broers, B., van Linden van den Heuvell, H., and Noordam, L. *Optics Communications* **91**(1.2), 57 – 61 (1992).

[17] Das, S. K., Schwanke, C., Pfuch, A., Seeber, W., Bock, M., Steinmeyer, G., Elsaesser, T., and Grunwald, R. *Opt. Express* **19**(18), 16985–16995 Aug (2011).

Appendix

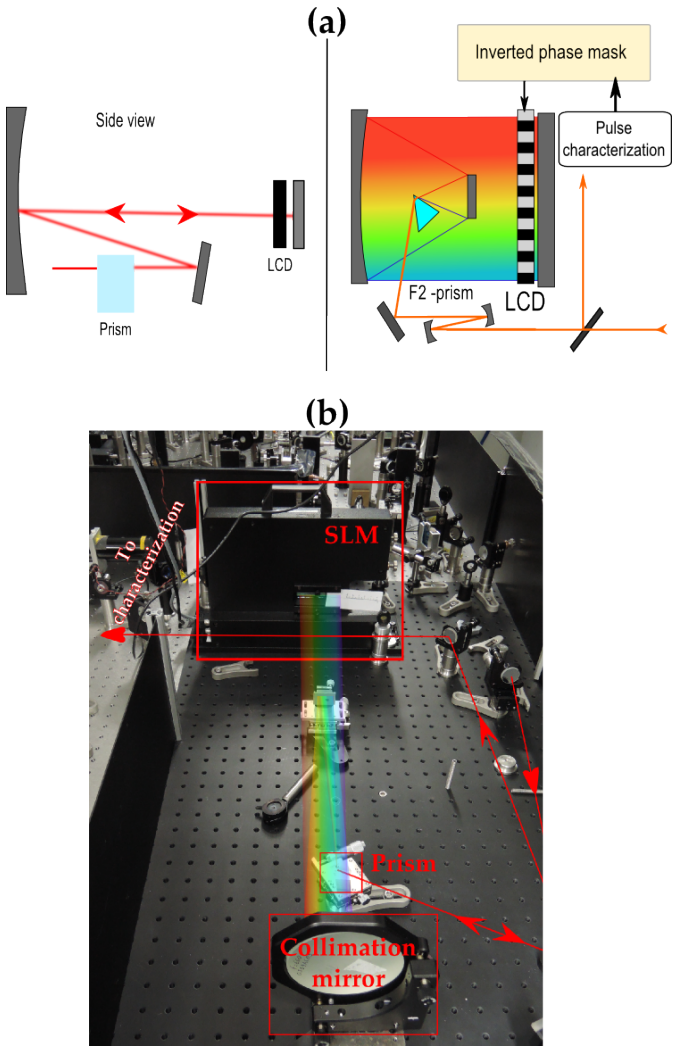

Figure 6: (a) Schematic (top and side view) of the used 4-f prism and SLM based shaper setup. It is in a folded geometry, and after characterization of the phase, this one is inverted and fed to the SLM for compensation. (b) Laboratorial implementation of the shaper. The main components are identified as well as an approximate beam path.

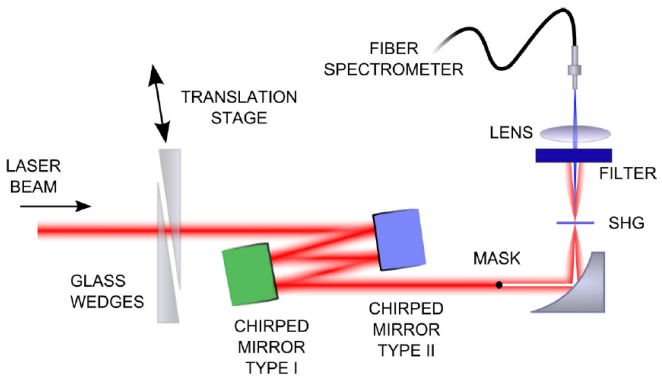

Figure 7: Schematic of a typical d-scan setup. The glass wedges are translated to impose different amounts of dispersion.